Interaction of spheres in oscillatory fluid flows

D. Klotsa, Michael R. Swift, R. M. Bowley, and P. J. King
School of Physics and Astronomy, University of Nottingham, Nottingham, NG7 2RD, United Kingdom
(Received 6 August 2007; published 19 November 2007)

Rigid spherical particles in oscillating fluid flows form interesting structures as a result of fluid mediated interactions. Here we show that spheres under horizontal vibration align themselves at right angles to the oscillation and sit with a gap between them. The details of this behavior have been investigated through experiments and simulations. We have carried out experiments in which a pair of stainless steel spheres is shaken horizontally in a cell filled with glycerol-water fluid mixtures of three different viscosities, at various frequencies and amplitudes of oscillation. There is an equilibrium gap between the particles resulting from a long-range attraction and a short-range repulsion. The size of the gap was found to depend on the fluid viscosity and the vibratory parameters, and we have identified two distinct scaling regimes for the dependence of the gap on the system parameters. Using a Navier-Stokes solver the same system was simulated. The interaction force between the spheres was measured and the streaming flows induced by the motion were determined.

DOI: 10.1103/PhysRevE.76.056314 PACS number(s): 47.55.Kf

I. INTRODUCTION

Granular systems are widespread in nature; the ability to understand and control their dynamical behavior is of central importance in many industrial processes [1]. A large number of granular phenomena occur as a result of the interaction between the grains and the fluid in which they are immersed, phenomena which range from simple sedimentation [2] to Faraday tilting [3,4] and stripe formation in oscillatory fluid flows [5]. However, the way in which rigid particles interact with each other within an oscillating fluid is still a challenging problem, involving as it does the nonlinear terms of the Navier-Stokes' equations.

The hydrodynamic interaction between isolated spheres in steady fluid flows is a well-known problem [6]. It can be solved analytically for low or high Reynolds' number, Re, by omitting either the inertial or the viscous terms from the Navier-Stokes' equations. Numerical methods have been used in the intermediate Re range where no term can be dropped [7,8]. The motion and flows of an isolated single sphere subjected to an oscillating fluid flow have also been studied both analytically and numerically [9–12]. In such a system there is a nonzero, time-averaged fluid flow around the sphere, called steady streaming, with two distinct regions of vorticity. It has been reported that when a single sphere is placed close to a boundary surface in the presence of an oscillating fluid flow, the sphere is attracted to the surface [13–15]. Other workers have found both an attractive and a repulsive force depending upon the sphere-surface separation [16]. The influence of the boundary on streaming flow patterns generated by spheres has also been investigated experimentally [17].

Recently, there has been an increasing interest in the interaction between a small number of spheres held in oscillatory fluid flows. Wunenburger *et al.* [18] have reported experiments in which small metal spheres were held in a shallow water-filled cell which was undergoing horizontal, sinusoidal vibration. The spheres were observed to form equally spaced chains, each oriented perpendicular to the direction of oscillation. Voth *et al.* [19] observed clusters and hexagonal lattices of lead spheres in a vertically vibrated cell filled with a glycerol-water mixture. Thomas and Gollub [20] studied the chaotic fluctuations of these clusters and concluded that the interparticle forces are not simply pairwise additive. A number of mechanisms, including the influence of steady streaming [18,19,21], have been proposed as the main source for these interactions. However, the exact details are still far from understood.

Here we present an experimental and computational study of the interaction between a pair of spherical metal spheres held in a liquid-filled cell which is undergoing horizontal vibration. Over a range of experimental conditions the spheres align themselves so that the line joining their centers is perpendicular to the direction of oscillation; they are spaced so that a gap is found between them. We investigate experimentally how the vibratory conditions and the fluid viscosity affect this spacing. The experimental results are compared with the predictions of a numerical model based on the Navier-Stokes' equations. The model allows us to investigate the spatial range of the interaction forces and to study in detail the fluid flow around the particles. We identify two distinct scaling regimes for the dependence of the gap on the system parameters and show how the scaling behavior is related to the streaming flow patterns generated by the spheres' motion.

II. EXPERIMENTAL DETAILS AND PRELIMINARY OBSERVATIONS

In all our experiments we used a liquid-filled cell formed by two 3 mm thick glass sheets. Each sheet was glued into an aluminum alloy frame. The two frames were separated by a butyl rubber gasket to form a liquid tight cell 135 mm long and 95 mm wide. The uniform spacing between the glass sheets could be varied but was set at 3 mm in the majority of the experiments reported below. The cell was mounted between two long-throw loudspeakers so that the plane of the glass sheets was accurately horizontal during vibratory mo-

tion and only one-dimensional motion in the horizontal plane occurred. The sinusoidal motion may be characterized by the frequency, f, and by the dimensionless acceleration of the cell, $\Gamma = A\omega^2/g$, which was determined using capacitive acceleration sensors. Here A is the amplitude of the vibration, $\omega = 2\pi f$ is the angular frequency, and g is the gravitational acceleration.

The experiments have been conducted using three different glycerol-water mixtures having kinematic viscosities $\nu = 2.0 \times 10^{-6}$ m^2 s^{-1}, 4.5×10^{-6} m^2 s^{-1}, and 9.4×10^{-6} m^2 s^{-1} at 22 °C. These mixtures have corresponding densities of 1060 kg m^{-3}, 1110 kg m^{-3}, and 1150 kg m^{-3}. The cell was filled with the selected liquid and sealed so that, ideally, no air was trapped in the cell. The laboratory temperature was controlled to avoid viscosity fluctuations.

In the majority of the experiments reported here the particles used were nonmagnetic, stainless-steel spheres, 1 mm in diameter and of density $\rho = 7950$ kg m^{-3}. An additional 1 mm diameter magnetic sphere was also placed in the cell. This sphere could be moved using a magnet positioned close to one of the glass sheets so that the pair under investigation could be repositioned. Alternatively, the magnetic sphere could be incorporated as one of the pair which could then be moved using the magnet. The principal results which we report here are for a pair of nonmagnetic spheres.

A high speed camera (up to 1000 frames per second) was mounted directly above the cell and the motion of the spheres was displayed on a monitor screen and recorded. In order to visualize the flow patterns of the liquid, we sometimes added marker particles to the solution [22]. Since the fluid viscosity is a strong function of temperature, the cell was force cooled with laboratory air when strong illumination was used.

In early experiments, small air bubbles formed in the cell under vigorous vibration. Their presence enabled us to observe that spheres do not roll appreciably during vibration, since the attached air bubbles maintain the same orientation with respect to the cell. This observation is in agreement with the calculations of Wunenburger [18] who concluded that, under oscillatory liquid flow, spheres slip on the bottom of the cell rather than roll. Since the source of these air bubbles was the air dissolved in the liquid, in the majority of our experiments the liquid was pumped just prior to use, using a rotary vacuum pump. The air bubbles did not then form.

Initially, a pair of spheres was placed in a liquid with $\nu = 2.0 \times 10^{-6}$ m^2 s^{-1}. Vibration at a frequency of 50 Hz and with $\Gamma = 5$ was then applied. The spheres rapidly attracted each other as soon as the vibration began, moving to sit with a small gap between them, their line of centers being perpendicular to the oscillation. The variation in this gap during each vibration cycle is very small. During their motion the spheres remain very close to the lower glass sheet. A pair of spheres will only interact and move to this equilibrium configuration if they are initially placed sufficiently close to one another. On the other hand, if the vibration begins when they are in contact, they repel one another and move to the same preferred configuration.

The alignment of the spheres perpendicular to the flow results from the oscillatory nature of the flow. Were one sphere to be displaced relative to the other in the flow direction, it would experience a greater drag force over part of the cycle, tending to bring it back into line. Over the second part of the cycle, the other sphere is also brought back into line.

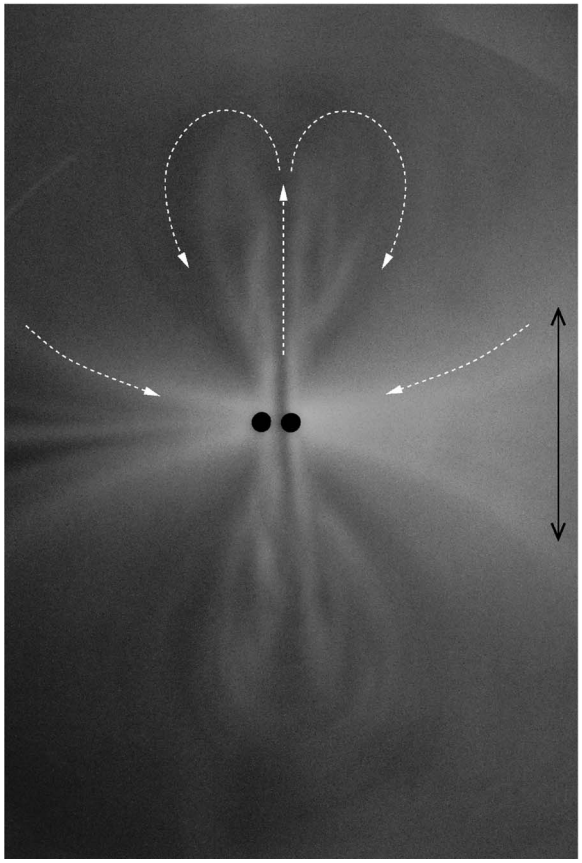

FIG. 1. Liquid flow patterns induced by a pair of 1 mm diameter spheres, in a cell vibrated at 50 Hz and with $\Gamma = 5$. The liquid used was a glycerol-water mixture with $\nu = 2.0 \times 10^{-6}$ m^2 s^{-1}. The white arrows indicate the direction of streaming flow on the upper side of the diagram; the flow on the lower side is the mirror image. The black, arrowed line indicates the direction of the oscillation.

The fluid movement induced by the spheres' motion could be inferred by observing marker particles. The movement consists principally of steady streaming flow. The form shown in Fig. 1 is typical: There is vigorous flow away from the spheres along the axis of vibration, the fluid returning along the orthogonal axis. The gap between the spheres is visible in the figure. Soon after the vibration is applied, fluid motion occurs close to the spheres. However, after a time of the order of tens of seconds this flow extends to many times the sphere diameter, as is also clear from the figure.

Wide ranging measurements of the gap were conducted. In our experiments the cell was vibrated within the range of frequencies 10–70 Hz and within a range of Γ between 1 and 9, corresponding to the amplitude A in the range 0.2–6.6 mm. For each frequency there is a range of values of Γ within which the interaction between the particles is strong and a stable gap may be observed. Below this range, the spheres drift apart, usually at an oblique angle to the direction of oscillation, indicating that the interaction is too weak

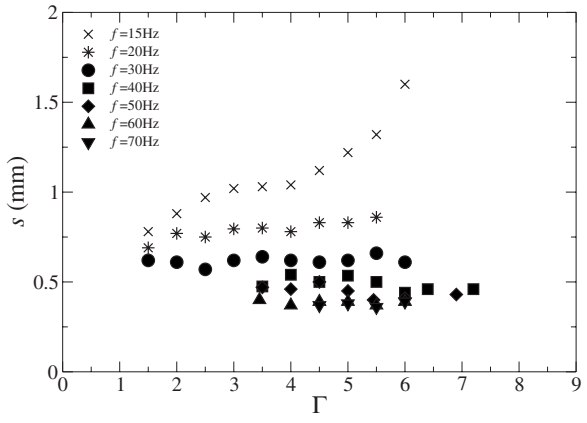

FIG. 2. Experimentally determined equilibrium gap, s, between a pair of 1 mm diameter spheres as a function of Γ for $\nu=9.4\times10^{-6}$ m^2 s^{-1}. The frequencies used are shown in the legend.

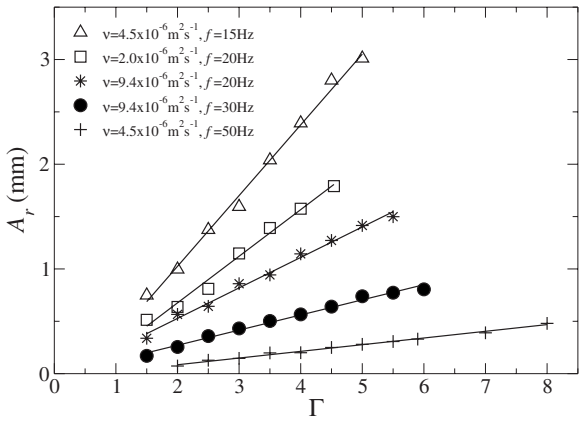

FIG. 4. Movement of the 1 mm diameter spheres relative to the cell, A_r, plotted against Γ for various values of the viscosity and frequency. The lines shown are best linear fits to the data.

to hold them at right angles to the oscillation. On the other hand, as the upper end of the range of Γ is approached, the motion of the spheres becomes increasingly erratic and the gap fluctuates. Beyond this upper limit the pair of spheres does not stay together.

The experiments were repeated using the more viscous fluids, with $\nu=4.5\times10^{-6}$ m^2 s^{-1} and 9.4×10^{-6} m^2 s^{-1}. Experiments were also conducted in which the cell spacing was varied, through the use of different thickness gaskets. It was found that the behavior depended very little on the cell spacing provided that the spacing is at least twice the sphere diameter. In all of the experiments reported here this condition is met.

III. RESULTS

First we report the variation of the equilibrium gap, s, with Γ, f, and ν. In Figs. 2 and 3, we show how s depends on Γ, for $\nu=9.4\times10^{-6}$ m^2 s^{-1} and for $\nu=4.5\times10^{-6}$ m^2 s^{-1}, respectively. It may be seen that, in each case, s grows rapidly with increasing Γ at low frequencies, but that the strength of this dependence falls rapidly with increasing frequency until at the highest frequencies studied there is very little dependence of s upon Γ. It is evident that the gap depends on viscosity since Figs. 2 and 3 differ. In these figures the scatter in the positions of the data points gives a good indication of the measurement errors.

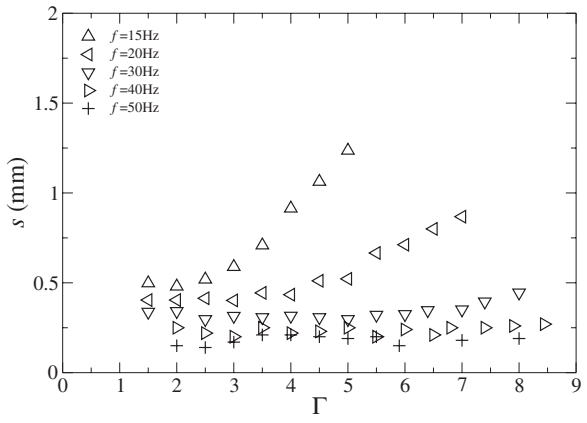

FIG. 3. Experimentally determined equilibrium gap, s, between a pair of 1 mm diameter spheres measured as a function of Γ for $\nu=4.5\times10^{-6}$ m^2 s^{-1}. The frequencies are shown in the legend.

A. Relative amplitudes

When a cell full of liquid is subjected to vibration, the liquid, being close to incompressible, moves with the cell. Since a sphere has a different density to the liquid, the sphere's inertia causes it to oscillate with respect to the cell and therefore with respect to distant liquid. In order to understand the motion of the spheres in detail, the *relative* amplitude of the spheres with respect to the cell, A_r, must be determined. For each of the viscosities used and for a range of values of f and Γ, we have filmed a number of cycles of oscillation of a pair of spheres and, from the camera images, we have determined A_r.

Figure 4 shows A_r plotted against Γ for a number of frequencies and viscosities. It may be seen that, in each case, the variation of A_r with Γ is very close to linear, with no sign of curvature at upper values of Γ. However, the sphere only moves with respect to the liquid when a critical value of Γ is exceeded, this value depending somewhat upon ν and ω. The data may be fitted by the expression

$$A_r = \frac{K(\nu,\omega)g}{\omega^2}[\Gamma - \Gamma_0(\nu,\omega)], \tag{1}$$

where $K(\nu,\omega)$ is a complicated function which varies slowly with ν and ω. The onset value, $\Gamma_0(\nu,\omega)$, lies typically in the range 0.2–0.8: It has a low dependence upon the viscosity, ν, but increases with increasing ω. The presence of an onset and its frequency dependence have been considered in detail by Wunenburger *et al.* [18] in terms of a model based on static friction and the viscous forces due to the translation and rotation of the sphere. Wunenburger *et al.*'s findings are consistent with our own observations. They conclude that for the values of Γ and ω considered here, each sphere slips

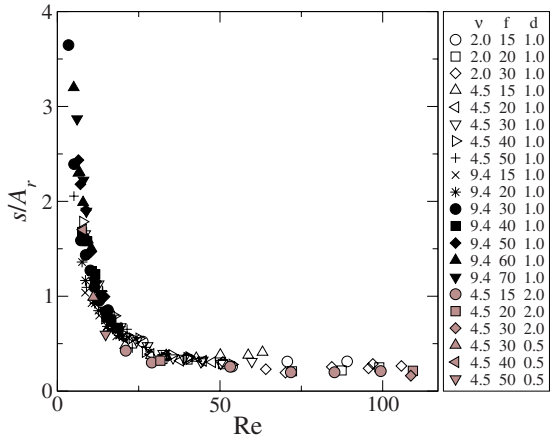

FIG. 5. (Color online) Collapse of the experimental data when plotted as s/A_r against the Reynolds number, Re, for the various viscosities, frequencies, and sphere diameters shown in the legend. In the table the viscosity ν is in units of 10^{-6} m^2 s^{-1}, the frequency f is in Hz, and the sphere diameter, d, is in units of mm.

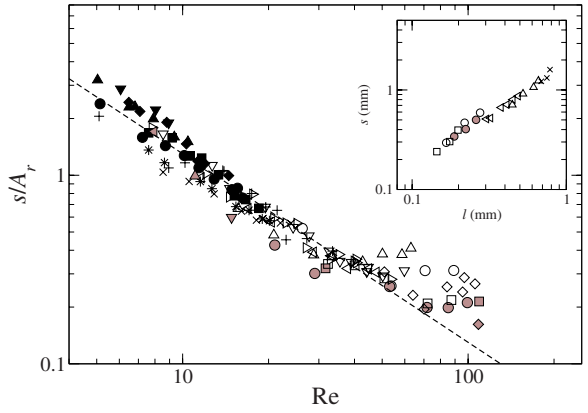

FIG. 6. (Color online) Collapse of the experimental data shown in Fig. 5 when replotted on a log-log scale. The dotted line is the fit described in the text. The collapse of the high Re data when the gap, s, is plotted versus $l=(A_r/d)\sqrt{\nu/\omega}$ is shown in the inset.

across the surface rather than rolling upon it, for almost all of the vibration cycle. Their observation is consistent with our own, that the motion of small air bubbles trapped on a sphere's surface indicates a lack of rotation.

B. Collapse of the data under scaling

We have seen that the equilibrium gap, s, between two spheres depends upon the frequency, f, the viscosity, ν, and upon the motion of the spheres relative to the cell, A_r. From additional experiments using spheres of diameters 0.5 and 2 mm we have also found that s is dependent upon the sphere diameter d. It is informative to determine whether dimensionless ratios of these parameters may be used to collapse the data. It is natural to select a Reynolds' number as one of these ratios; we use $\mathrm{Re}=A_r\omega d/\nu$. In our studies, Re ranges between about 5 and 120, a range intermediate between laminar flow and full turbulence, whereas the sphere size ranges over a factor of 4 and the viscosity and frequency each vary by a factor of 5. If A_r is used to scale the gap and s/A_r is plotted versus Re, it is found that the data lies close to a single curve. This collapse is shown in Fig. 5. Figure 6 shows the same collapse plotted on a log-log scale. Most of the data lies reasonably close to a line with a gradient of −1.0. This data may therefore be described approximately by the relationship $s=C\nu/(\omega d)$, where C is a numerical constant. A fit using the value $C=13\pm1$ is shown as the broken line in the figure. It is noteworthy therefore that, for this data, the equilibrium separation does not depend upon A_r.

It may also be seen from Fig. 6 that some of the data at higher values of Re do not scale in the way we have just described, the data points lying well above the broken line. The distinction between the two classes of data is very evident from Figs. 2 and 3. The data which undergoes the scaling collapse which we have just described occurs for higher frequencies where the gap is not dependent upon Γ and thus upon A_r. However, these figures show that at the lowest frequencies, where A_r is large, the gap is extremely dependent both upon A_r and also upon frequency; the dependence upon A_r disappears very quickly as the frequency is raised. It is this lower frequency data, corresponding to the high Re data of Fig. 6, which does not undergo the scaling collapse just described. However, this data may be collapsed by plotting the gap, s, against $l=(A_r/d)\sqrt{\nu/\omega}$ as may be seen in the inset of Fig. 6. On this log-log plot the collapse is close in form to a straight line with gradient of unity. For this data, therefore, $s\approx C'(A_r/d)\sqrt{\nu/\omega}$, where C' is a constant equal to 1.8 ± 0.2.

The crossover from one form of scaling to the other is relatively abrupt. The condition for the crossover may be obtained by equating the gaps in two scaling regimes. This gives the condition $A_r=(C/C')\sqrt{\nu/\omega}\approx7\sqrt{\nu/\omega}$. We note that the length $(\nu/\omega)^{1/2}$ is the oscillatory boundary layer parameter associated with streaming flow [23].

It is also interesting to note that, in the low amplitude regime, the gap scales in the same way as the distance of the stagnation point from the surface, for streaming flows around an isolated sphere [24].

IV. COMPUTER SIMULATIONS

To gain insight into the physical mechanisms which lead to the formation of a gap, and in order to be able to study features not readily accessible from experiment, we have also carried out numerical simulations. The fluid and the spheres are modeled using a simplified version of the method developed by Kalthoff *et al.* [25]. The fluid is assumed to be incompressible and described by the 3D Navier-Stokes' equations

$$\frac{\partial \mathbf{v}}{\partial t}+(\mathbf{v}\cdot\boldsymbol{\nabla})\mathbf{v}=-\frac{1}{\rho}\nabla P+\nu\boldsymbol{\nabla}^2\mathbf{v}-\mathbf{g}, \tag{2}$$

$$\boldsymbol{\nabla}\cdot\mathbf{v}=0. \tag{3}$$

Here $\mathbf{v}$ is the fluid velocity, P is the fluid pressure, ρ is the fluid density, and $\mathbf{g}$ is the acceleration due to gravity. These equations are discretized on a staggered marker and cell (MAC) mesh [26] and solved using the projection method [27].

The spheres are treated as solid objects surrounded by the fluid, and the fluid-solid coupling is introduced by enforcing the no-slip boundary condition on the surface of the spheres. This is achieved numerically by representing the spheres as fluid moving with the instantaneous sphere velocity. At each time step, the spheres' velocities are transferred to the fluid at the sites occupied by the spheres and the fluid evolves under the Navier-Stokes' equations, ensuring that the continuity equation is satisfied. The force on each sphere, **F**, is then calculated from

$$\mathbf{F} = \sum_i (-\nabla P + \nu\rho\nabla^2\mathbf{v}), \tag{4}$$

where the sum is over all fluid sites occupied by a sphere and the derivatives are calculated using finite difference approximations. This force is then used to update the spheres' positions using molecular dynamics techniques [28]. Full details of the method can be found in [29].

Our 3D Navier-Stokes' solver simulates motion of the fluid and particles in a container of dimensions 21 mm $\times$10.5 mm$\times$3 mm. The grid size used was $\Delta x = 7.5 \times 10^{-5}$ m, giving a system of size $280\times140\times40$ lattice points. The spheres, typically 1 mm in diameter, occupy about 1200 lattice points. A time step of $\Delta t = 10^{-6}$ s was used throughout. All other fluid and particle parameters were chosen to be the same as in the experimental systems described above. As in experiments, the spheres are influenced by gravity in the vertical direction, aligned perpendicular to the largest faces of the container. As a result, the spheres ride on the lower surface. However, to avoid the complications associated with lubrication forces, the spheres are prevented from reaching the outer cells of the fluid grid by a contact force which restrains them to be at least one lattice spacing from the true cell boundary.

If, in simulation, the fluid-particle system is subjected to horizontal oscillation, the spheres are found to align perpendicular to the flow direction and to sit at a well defined spacing, as observed experimentally. However, as we have not dealt fully with the interaction with the surface, which is known to be complex [18], the simulated relative amplitude A_r is somewhat different from the experimentally measured value for a given set of driving conditions. In order to make a more direct comparison with experiment, while keeping the model computationally simple, we have proceeded as follows.

Initially the fluid is at rest and the spheres are positioned across the cell at a spacing $s=d$. While maintaining the walls of the cell at rest, both spheres are then oscillated along the longest horizontal dimension of the cell as $A_r \sin(\omega t)$, using the experimentally measured values of A_r appropriate to the particular parameters being used. The fluid moves in response to the spheres' motion while the spheres are free to move without rotation, vertically and along the line joining their centers, under the influence of the fluid force, gravity, and the surface contact force in the vertical direction. In practice, we find little movement in the vertical direction, the spheres remaining one grid cell from the lower surface during their motion. Each simulation is continued until a steady gap and an equilibrium fluid flow pattern is achieved.

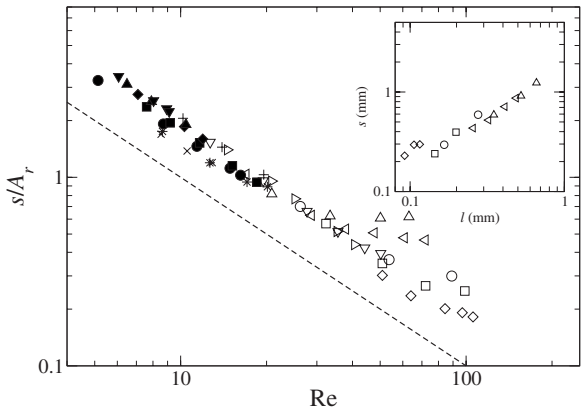

FIG. 7. Scaling collapse of the simulation data, presented in the same way as the experimental data shown in Fig. 6. The symbols correspond to the system parameters given in the legend to Fig. 5. The dashed line indicates the mean position of the experimental data.

A. Estimates of the gap from simulations

We find that the simple simulation technique which we have described above is able to capture the principle feature of the phenomena observed in experiment: A pair of spheres displays a gap which depends upon the system parameters. Figure 7 shows simulation data for the equilibrium gap presented in the same way as the experimental data in Fig. 6. The similarity is evident. When plotted as s/A_r versus Re, on a log-log plot, the lower amplitude simulation data falls on a straight line with a gradient close to -1. For this simulation data the constant C is close to 18. As in experiment, the higher amplitude data scales differently, the inset showing its behavior. For this simulation data the constant C' is close to 1.8. Although C' is the same as the corresponding value for the experimental data, the constant C is somewhat higher in simulation. For comparison, the mean position of the experimental data is shown in Fig. 7 as the broken line. The simulation data also show a relatively abrupt transition from one scaling regime to the other, the transition occurring when $A_r \approx 10\sqrt{\nu/\omega}$. Here the numerical constant is greater than from experiment, because of the higher value of C.

We believe that the discrepancy between the simulated gap data and the corresponding experimental data is partly due to the way we have treated the interaction of the spheres with the surface and partly due to computational limitations. As stated above, we have constrained the bottom of the spheres to remain at least one lattice spacing above the lower surface of the cell. We note that if the spheres are held further above the lower surface, the agreement with experiment is not as good, due to the influence of the lower surface on the streaming flow. We therefore infer that better agreement could be obtained if the spheres were brought closer to the surface by reducing the lattice size. However, such a refinement becomes increasingly computationally prohibitive.

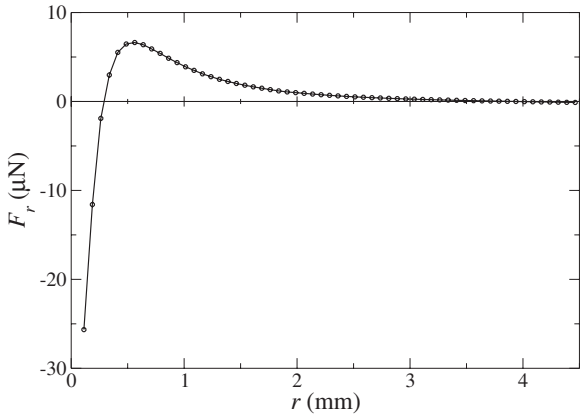

FIG. 8. Interaction force, F_r, as a function of the space between the spheres, r, for a pair of spheres vibrated at 50 Hz with A_r =0.28 mm in a fluid of viscosity 4.5×10^{-6} m^2 s^{-1}. The corresponding Re is approximately 20.

Nevertheless, it is clear that the simple model given here is able to capture, semiquantitatively, the main features of the experimental observations, giving us the confidence to use our model to investigate the fluid-driven mechanisms responsible for the gap.

B. Force measurements

From simulation, it is possible to determine the forces on the spheres due to their motion with respect to the surrounding fluid. We will consider the force on one sphere in the direction of the other, F_r, as a function of the spacing between the spheres, r. This can be obtained by keeping the spheres at a fixed separation while oscillating them in the direction perpendicular to the line joining their centers. The time-averaged force as a function of separation is shown in Fig. 8 for a typical set of driving conditions.

At large separations the force is attractive, whereas at small separations it becomes repulsive. The separation for which the force is zero corresponds to the equilibrium gap described above. At large separations the attractive force decays approximately as $r^{-\alpha}$, with α close to 2. As Re is reduced, this attraction becomes increasingly weak.

C. Fluid flows

The simulations also allow us to determine the fluid flows generated by the oscillatory motion of the spheres. Here we consider the time-averaged streaming component of the flow, obtained by averaging the flow over one cycle of vibration once an equilibrium flow pattern has been reached. In simulation, the flow is generated by moving the spheres in a static box. However, for clarity, we will present the streaming flow field relative to the spheres. For our container geometry, the flow is predominantly two dimensional. This is in agreement with the experimental finding that the behavior is not dependent on the spacing between the upper and lower plates, provided that the spacing is greater than about two particle diameters.

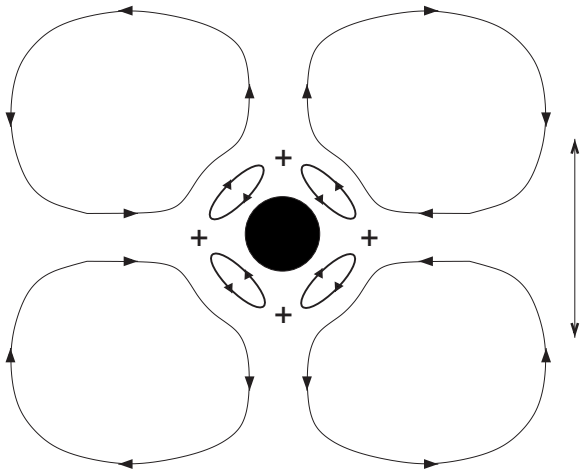

FIG. 9. Schematic diagram showing streaming flow around a single isolated sphere. The arrowed straight line shows the direction of oscillation. The crosses correspond to stagnation points.

The streaming flow generated by a *single isolated sphere* is well known [10]. It typically consists of two *inner* vortex loops with flow away from the sphere at the equator, and two *outer* vortex loops with flow in toward the sphere at the equator. A 2D slice through such a streaming flow pattern, perpendicular to the equatorial plane and through the center of the sphere, shows four inner vortices and four outer vortices, as illustrated schematically in Fig. 9. For small amplitude, low Re, oscillation, the inner vortices dominate and the outer vortices are extremely weak. As Re increases, the inner vortices shrink in size and the outer vortices strengthen [10,30,31]. It should be noted that the instantaneous fluid flow has only one inner vortex loop which oscillates backward and forward around the sphere; the outer loops are always present.

For a *pair of spheres* in our cell geometry, we have identified two distinct streaming flow patterns, corresponding to the two different scaling regimes discussed above. Figures 10(a) and 10(b) show these flow diagrams at low and high amplitudes, respectively. These slices are taken through the center of the spheres, parallel to the lower surface of the container. In each case the sphere separation is fixed at its equilibrium value. For low amplitudes, the flow is dominated by eight inner vortices close to the spheres. The flow around each sphere is similar in structure to that expected for a single sphere in isolation. However, the vortices close to the gap are smaller than they would be for an isolated sphere. Away from the spheres, the outer streaming flow is very weak indeed.

In contrast, at high amplitudes, the dominant flow is associated with the outer vortices. The eight inner vortices close to the spheres are still present. However, there are only four outer vortices, shown in Fig. 10(b), rather than the eight which would be expected for two spheres in isolation. This outer vortex pattern for the pair of spheres is similar to that of a *single* sphere; however, the outward flow is now centered on the gap rather than on the poles of the spheres. Because of the shift in the position of the outward flow, the circulation of the inner vortices within the gap strengthens

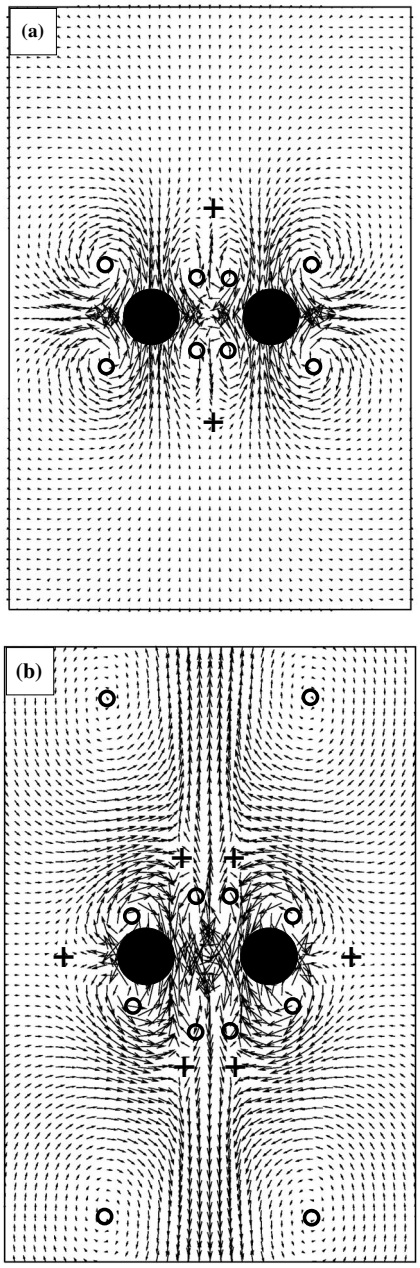

FIG. 10. Vector plot taken from numerical simulation of the average fluid flow for two 1 mm spheres at their equilibrium gap. The system parameters used are (a) $\Gamma=6.0$, $f=40$ Hz, and $\nu=9.4\times10^{-6}$ m^2 s^{-1} and (b) $\Gamma=4.5$, $f=20$ Hz, and $\nu=2.0\times10^{-6}$ m^2 s^{-1}. The open circles indicate the centers of vortices while the crosses mark stagnation points.

this outward flow, resulting in strong jets of fluid flowing away from the gap. We have observed this behavior experimentally; an example is shown in Fig. 1.

As the vibration parameters are varied from one regime to the other, the streaming pattern crosses over from one form to the other. This behavior is shown schematically in Fig. 11, for parameters spanning the crossover region. Figure 11(a) shows the low-amplitude behavior. The inner vortices close to the gap are relatively weak and there is a stagnation point nearby. As the amplitude increases, the inner vortices close

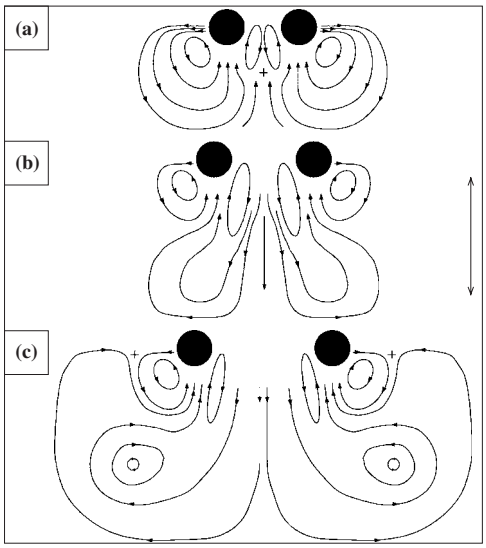

FIG. 11. Schematic diagram showing streaming flow around two spheres for (a) low amplitude ($\Gamma=2$), (b) intermediate amplitude ($\Gamma=3$), and (c) high amplitude ($\Gamma=4$). The figures are based on simulations carried out at 50 Hz and with $\nu=4.5\times10^{-6}$ m^2 s^{-1}. For clarity we have only drawn the lower streamlines. The arrowed line on the right indicates the direction of oscillation.

to the gap increase in magnitude and spatial extent, and the stagnation point moves away. The resulting flow is shown in Fig. 11(b). At yet higher amplitudes, the outflow from the gap is sufficiently strong to generate large outer vortices, as shown in Fig. 11(c). The outflow now can return along a line joining the center of the spheres, until it approaches the stagnation point. As far as we can tell there is a smooth transition from one regime to the other.

V. DISCUSSION

We have shown that two spheres subjected to oscillatory fluid flow will attract each other and line up across the flow with a well-defined equilibrium gap between them. From both experiment and simulation we have identified two distinct dependencies of the gap on the system parameters. Simulations also show that the force between the spheres is attractive at large separations and repulsive for short separations. It is the balance between the attractive and repulsive parts of the force that gives rise to the equilibrium gap.

What are the possible causes of the repulsion and attraction? Simulations suggest that the repulsion at short separations arises from the overlap of the inner vortices within the gap, which tend to drive the particles apart. At large separations, the attractive nature of the interaction may result from the inflow associated with the outer streaming around a single sphere, as suggested in Refs. [18,19,21]. However, at shorter separations, we still find an attractive force in simulations, even though there is no observable inflow. An

understanding of this behavior based simply on streaming flows may not be possible.

Despite the lack of a complete understanding of the forces involved, the present work has shed some light on the complex nature of the interaction between particles in oscillatory fluid flows.

ACKNOWLEDGMENTS

We are grateful to the Engineering and Physical Sciences Research Council for support, and to the workshop staff of the School of Physics and Astronomy for their skills and enthusiasm.

[1] H. M. Jaeger, S. R. Nagel, and R. P. Behringer, Rev. Mod. Phys. **68**, 1259 (1996).
[2] For a review, see S. Ramaswamy, Adv. Phys. **50**, 297 (2001).
[3] M. Faraday, Philos. Trans. R. Soc. London **52**, 299 (1831).
[4] R. J. Milburn, M. A. Naylor, A. J. Smith, M. C. Leaper, K. Good, M. R. Swift, and P. J. King, Phys. Rev. E **71**, 011308 (2005).
[5] P. Sanchez, M. R. Swift, and P. J. King, Phys. Rev. Lett. **93**, 184302 (2004).
[6] For a review, see J. F. Brady and G. Bossis, Annu. Rev. Fluid Mech. **20**, 111 (1988).
[7] I. Kim, S. Elghobashi, and W. A. Sirignano, J. Fluid Mech. **246**, 465 (1993).
[8] R. Folkersma, H. N. Stein, and F. N. van de Vosse, Int. J. Multiphase Flow **26**, 877 (2000).
[9] N. Riley, Annu. Rev. Fluid Mech. **33**, 43 (2001).
[10] N. Riley, Q. J. Mech. Appl. Math. **19**, 461 (1966).
[11] H. M. Blackburn, Phys. Fluids **14**, 3997 (2002).
[12] R. S. Alassar and H. M. Badr, Comput. Fluids **26**, 661 (1997).
[13] S. Hassan, T. P. Lyubimova, D. V. Lyubimov, and M. Kawaji, Trans. ASME, J. Appl. Mech. **73**, 72 (2006).
[14] S. Hassan, T. P. Lyubimova, D. V. Lyubimov, and M. Kawaji, Int. J. Multiphase Flow **32**, 1037 (2006).
[15] D. V. Lyubimov, A. A. Cherepanov, T. P. Lyubimova, and B. Roux, J. Phys. IV **11**, 83 (2001).
[16] A. A. Ivanova, V. G. Kozlov, and A. F. Kuzaev, Dokl. Akad. Nauk **402**, 488 (2005) [Dokl. Phys. **50**, 311 (2005)].
[17] F. Otto, E. K. Riegler, and G. A. Voth, e-print arXiv:0709.4305v1[cond-mat.soft].
[18] R. Wunenburger, V. Carrier, and Y. Garrabos, Phys. Fluids **14**, 2350 (2002).
[19] G. A. Voth, B. Bigger, M. R. Buckley, W. Losert, M. P. Brenner, H. A. Stone, and J. P. Gollub, Phys. Rev. Lett. **88**, 234301 (2002).
[20] C. C. Thomas and J. P. Gollub, Phys. Rev. E **70**, 061305 (2004).
[21] L. Petit and P. Gondret, J. Phys. II **2**, 2115 (1992).
[22] Kalliroscope Corporation, www.kalliroscope.com
[23] G. K. Batchelor, *An Introduction to Fluid Dynamics* (Cambridge University Press, Cambridge, UK, 1967).
[24] C. K. Kotas, M. Yoda, and P. H. Rogers, Exp. Fluids **42**, 111 (2007).
[25] W. Kalthoff, S. Schwarzer, and H. J. Herrmann, Phys. Rev. E **56**, 2234 (1997).
[26] F. H. Harlow and J. E. Welch, Phys. Fluids **8**, 2182 (1965).
[27] K. Höfler and S. Schwarzer, Phys. Rev. E **61**, 7146 (2000).
[28] M. P. Allen and D. J. Tildesley, *Computer Simulations of Liquids* (Clarendon Press, Oxford, 1987).
[29] R. Milburn, Ph.D. thesis, School of Physics and Astronomy, University of Nottingham, 2006.
[30] J. M. Andres and U. Ingard, J. Acoust. Soc. Am. **25**, 932 (1953).
[31] J. M. Andres and U. Ingard, J. Acoust. Soc. Am. **25**, 928 (1953).